fortune Journals

Review Article

JOURNAL OF BIOTECHNOLOGY AND BIOMEDICINE

ISSN: 2642-9128

L-shell X-ray Production Cross Sections Induced by Carbon Ions: A Review

Ernest Ejeh[1*], Morgan Madhuku[1], Faith Ochai-Ejeh[2], Audu Innocent[3], Philip Sechogela[1]

Abstract

This review presents a comprehensive and critical analysis of L-shell X-ray production cross sections (XRPCS) induced by carbon ions in the MeV range, spanning a 23-year period from 2000 to 2023. The accurate determination of X-ray production cross sections holds significant importance in diverse applications, including Particle-Induced X-ray Emission (PIXE), molecular and atomic physics, the development of new ion-atom collision theories, and the enhancement of existing ones that are currently trailing. This review focuses on recent advancements in XRPCS associated with carbon ions, particularly in the realm of heavy ion PIXE (HI-PIXE) applications within various scientific and biological domains. A thorough examination is undertaken to compare and contrast experimental data with established theories, including but not limited to PWBA, ECPSSR, ECUSAR, FBA, and SCA.

Keywords: L-shell; X-ray production cross section; PIXE; Ionization; Carbon; ECPSSR; Heavy- ions

Introduction

Inner shell ionization cross sections of targets induced by charged particles have been the focus of extensive research with in-depth experimental and theoretical investigations spanning several decades. The study of inner shell ionization is crucial, as it plays a fundamental role in developing new models for ion beam-atom interactions. Additionally, it provides essential physical cross- sectional data for the development and implementation of ion beam analysis techniques, the calculation of stopping powers, the study of solids and plasmas, and for building databases for applications such as Particle-Induced X-ray Emission (PIXE) [1-3]. PIXE is an accelerator- based ion beam technique used to study the qualitative and quantitative properties of samples by exciting characteristic X-rays due to the impact of charged ions. The qualitative aspect of PIXE involves identifying elements in the sample based on the energy of characteristic peaks in the X- ray emission spectrum, while the quantitative aspect involves determining the quantity of a particular element present in the sample from the intensity of the X-ray emission spectrum (See Figure 1).

Both qualitative and quantitative aspects can be measured readily, as a single run simultaneously determines them, enabling rapid detection of many elements, including trace elements. PIXE's versatility has addressed challenges in various scientific fields, including geology, biomedicine, environmental science, biology, nuclear science, forensics, archaeology, and industry [4-8]. It has been employed to analyze a variety of materials, including biological samples, water, soil, wood, aerosols, artifacts, hair, urine, plasma, and pleural effusion [9-11]. Using this technique, the elemental concentration of nearly

Affiliation:
[1]iThemba LABS TAMS, National Research Foundation, Johannesburg, South Africa.

[2]Department of Physics and Astronomy, University of Nigeria, Nsukka, Enugu State, Nigeria.

[3]Department of Science Education, University of Brighton, United Kingdom.

***Corresponding author:**
Ernest Ejeh, iThemba LABS TAMS, National Research Foundation, Johannesburg, South Africa.

Citation: Ernest Ejeh, Morgan Madhuku, Faith Ochai-Ejeh, Audu Innocent, Philip Sechogela. L-shell X-ray Production Cross Sections Induced by Carbon Ions: A Review. Journal of Biotechnology and Biomedicine. 7 (2024): 471-484

Received: September 20, 2024
Accepted: October 14, 2024
Published: November 28, 2024

all elements in the target, typically ranging from aluminum to uranium can be determined through the measurement of X-ray yields from various atomic shells (K-M). Additionally, detailed spatial information about the elements can be obtained using the PIXE micro-beam system [6,12-15].

PIXE studies are typically conducted using accelerated light ions such as protons and helium in the 1-3 MeV energy range [16-24]. Numerous literature reviews on K shell, L shell ionization, and X-ray production cross sections (XRPCS) for a wide range of elements due to the impact of light ions have been published [4,25-29]. These reviews have facilitated the development of comprehensive light ion databases, promoting light ion PIXE measurements. Furthermore, inner shell ionization induced by light ions is often a single-ionization process. As a result, multielectron processes in ion-atom interactions can be disregarded in their analysis, except in cases where the transferred energy is high enough to remove more than one electron from the atom.

One enduring aspect of science is the continual evolution of scientific knowledge. In PIXE measurements, there has been a notable shift towards using heavy ions due to the observed enhanced sensitivity and larger X-ray yields emitted when heavy ions serve as projectiles [8,29-31]. These authors (refer to references [8, 29-31] emphasized that despite the clear advantages of employing heavy ions, it is crucial to first understand the ion-atom mechanisms involved when heavy ions are used. This understanding is essential for obtaining valid results from Heavy Ion PIXE (HI-PIXE) measurements. To enhance the global database for HI-PIXE analyses and applications, ongoing research and reviews on ionization cross sections and X-ray production cross sections by heavy ions are essential.

Among heavy ions used in PIXE-related measurements and analysis, carbon ions are the most widely utilized. In the work of Mehta et al. [32], out of the fifteen surveyed published data on L shell X-ray production cross section (XRPCS) induced by heavy ions, nine focused on carbon ions. Underscoring the importance of carbon ions, high-energy carbon ions have found application in the treatment of cancer tumors in medicine and medical physics. Medical physicists, radiation oncologists, and radiobiologists have reported that carbon ions yield excellent results and offer significant advantages over protons. These advantages include a better physical dose distribution, higher relative biological effectiveness, and lower oxygen enhancement in the control and treatment of non-invasive deep-seated cancers [33-37]. Existing literature demonstrates a consistent agreement between experimental data and theoretical predictions when carbon ions are employed [4,8,38]. Orlic et al. [39] underscored the importance of compiling experimental L shell ionization cross-section data to promote further measurements in this area. While additional research on heavy ion-induced L shell X-ray production cross-section is warranted [14,39,40], it is advisable to conduct a comprehensive review study on heavy ions X-ray production cross-sections. Such a review would elucidate the progress made and encourage the full implementation of Heavy Ion PIXE (HI-PIXE) applications in scientific and biological fields.

This work presents a modest review on L-shell X-ray production cross sections (XRPCS) induced by carbon ions. The remainder of this paper is organized as follows: Section 2 will cover heavy ion cross-sections, Section 3 will address the effect of heavy ions on X-ray production cross- sections, and Section 4 will focus on the comparison between experimental data and theoretical predictions in ion-atom collisions.

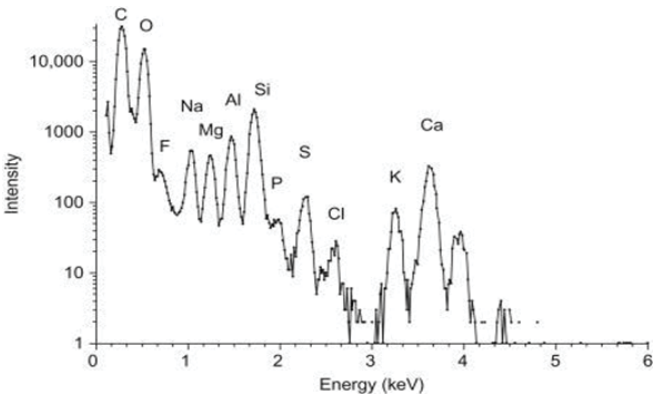

Figure 1: X-ray spectrum of an aerosol sample [41].

Heavy Ion Ionization Cross Section

When a heavy ion collides with a target, the scattering phenomenon is described by a quantity called cross-section. Gudennavar et al. [42], define cross section as the probability that a particular time-dependent process will occur. Therefore, the probability that the interaction of an ion with a target material will result in atomic ionization is termed ionization cross-section, estimating the number of ionizations that will occur in a collision. Ionization cross-section from a target depends on (i) the atomic number of the incident ion Z_1 (ii) the velocity of the ion v_1 and (iii) the velocity of the inner electron of the target atom v_2. When electrons, protons, and photons serve as projectiles, single inner-shell vacancies are produced. However, in the case when a heavy ion (Z1> 2) is used as a projectile, there is a high probability that additional electrons will be ejected during the inner-shell ionization process—a term known as multiple ionization (detailed discussion in Section 3). The removal of electrons increases the binding energies of the remaining electrons due to the reduction of the screening of the nuclear charge felt by the remaining electrons.

Each ionization process is characterized by different collision parameters that determine the mechanism through

Ejeh E, et al., J Biotechnol Biomed 2024
DOI:10.26502/jbb.2642-91280170

which inner shell vacancies are produced. Two main processes are responsible for inner shell vacancies in heavy ion collisions: direct ionization (DI) and electron capture (EC). The DI mechanism is pronounced when $Z_1 \ll Z_2$ and $v_1 \gg v_{2s}$, while the EC mechanism dominates when $Z_1 \leq Z_2$ and $v_1 \leq v_{2s}$ where Z_1 and Z_2 are the atomic numbers of the projectile and the target atom respectively, v_1 and v_{2s} are the velocities of the projectile and the target inner- shell (S = K-shell, L-shell) electrons, respectively. Electron capture (EC) involves the capturing of electrons from the inner shell of a target by the projectile creating a vacancy in the inner K-shell especially for symmetric collision. An increase in the projectile energy increases the probability of EC [43,44].

X-ray Production Cross Section

The X-ray production cross-section is a physical quantity that depends on several factors, such as the projectile, energy, and the target atom. It represents the probability of producing X-ray photons of a particular line. Orlic et al. [39] recommend using X-ray production cross sections due to conversion errors between X-ray ray production cross sections and ionization cross sections. We therefore focusing on X-ray production cross sections in this review. Equations (1-3) can be used to calculate the L X-ray production cross sections of common lines, as reported in [45]:

$$\sigma_{X,}L_l = (\sigma_{L1}f_{13} + \sigma_{L1}f_{12}f_{23} + (\sigma_{L2}f_{23} + \sigma_{L3})\omega_3 F_{3l} \quad (1)$$

$$\sigma_{X,}L_\beta = \sigma_{L1}\,\omega_1 F_{1\beta} + (\,\sigma_{L1}f_{12} + \sigma_{L2})\omega_2 F_{2\beta} +$$

$$(\sigma_{L2}f_{13} + \sigma_{L2}f_{23} + \,\sigma_{L2})\omega_3 F_{3l}, \text{ and} \quad (2)$$

$$\sigma_{X,}L_\gamma = \sigma_{L1}\omega_1 f_{1\gamma} + (\sigma_{L1}f_{12} \,+ \sigma_{L2})\omega_2 F_{2\gamma} \quad (3)$$

Where, the σ_{Li} are the ionization cross sections of an individual Li subshell, ω_i is the fluorescence yield of the i subshell, f_{ij} is the probability for a Coster-Kronig transition between subshells i and j, while F_{nx} is the probability of producing a radiative transition, taken as the fraction of X-ray photons originated from a vacancy in the Ln subshell, contributing to the F_{nx} line.

Heavy Ion Effect on X-ray Production Cross Sections

When heavy ions are used as incident ions, targets experience significantly more complex effects, such as multiple ionization, compared to when light ions are used [45-48]. These effects are dependent on the atomic number of the ion, meaning the gravity of the complexity [47,49] increases with atomic number [4,46].

Multiple Ionization Effects by Heavy Ion Impact

The collision of high-energy ions with atoms can induce a phenomenon called multiple ionization (MI), where the intense electric field of the incident ion triggers the simultaneous ejection of multiple electrons from the atom [6], signifying the probability of creating more than one vacancy in a single collision event [8]. In bridging the gap between ion-atom interaction theories and experiments, multiple ionization becomes a critical factor, especially when heavy energetic ions serve as the probing projectiles. This is because they can induce the creation of multiple vacancies, particularly within the inner (K-L) shells, which significantly affects the interaction dynamics. Raju et al. [50] demonstrated that MI causes discrepancies between theoretical predictions and experimental results even when using lighter ions, such as protons. Lapicki et al. [50] reviewed numerous studies [18,36,41-61] investigating the effects of multiple ionization (MI). These studies discussed and addressed the various complexities associated with MI. Multiple ionization can lead to changes in:

(i) Fluorescence yield values and Coster-Kronig transitions (ii) Electron binding energies (i.e., X- ray line shifts and broadening, (See Figure 2)) and (iii) X-ray intensity ratios (as shown in Figure 2).

These effects occur due to vacancy rearrangement between the initial ion collision and subsequent X-ray emission. To bridge the gap between theoretical and experimental findings, a careful correction for these MI-induced effects is essential [4,6].

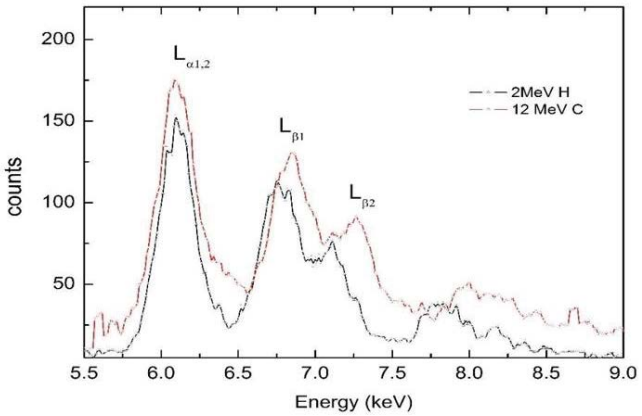

Figure 2: Multiple ionization effect on gadolinium L-shell X-ray energies due to 12 MeV carbon projectiles [4].

Fluorescence Yield and Coster-Kronig Transition

Benka et al. [51] demonstrated that discrepancies between experiments and theoretical X-ray production cross-sections can be attributed to uncertainties in the atomic parameters associated with the inner shell. There is a high probability that multiple ionization (MI) can cause the ionization of the outer shell of the atomic target, resulting in increased fluorescence yields for singly ionized atoms and a subsequent reduction in the probability of Auger transition [51]. A report by Banás et al. [52] highlighted that one of the most pronounced effects

Ejeh E, et al., J Biotechnol Biomed 2024
DOI:10.26502/jbb.2642-91280170

of multiple ionization (MI) is the closing or reduction of some Coster-Kronig transitions. This process increases the fluorescence yield, leading to a significant rise in theoretical X-ray production cross- sections. However, it is important to note that fluorescence yield also decreases with a decrease in projectile velocity and complicates the resolution of individual X-ray transitions [53]. Coster- Kronig transitions are radiationless transitions in which the inner shell vacancy of an atom is filled by an electron from a higher subshell of the same principal shell.

During an ion-target atom collision, the target atom can undergo a change in the atomic parameters as a result of MI resulting in multiple vacancies (MV), which in turn lead to increase in the fluorescence yield (FY) w_i^0, a decrease in Coster-Kronig transition (CK) $f_{ij}{}^0$, and the Auger transition affecting the X-ray production sections. Considering these effects, Czarnota et al. [54] emphasized the importance of careful selection of atomic parameters in theoretical calculations of L-subshell X-ray production cross sections.

One of the most used correction model for single-hole fluorescence w^0 and Coster-Kroning $f_{ij}{}^0$, is a model proposed by Lapicki et al. [50]. We shall focus on the model for the purpose of this review. This model corrects an increase in single hole fluorescence yield (FY) w^0 and a subsequent decrease in Coster-Kronig transition (CK) $f_{ij}{}^0$, due to multiple ionization. They assume that ionization probability of each electron among several other subshells is P. Using the same factor of 1-P for all radiative factor widths, including all Auger rates involving two electrons in the manifold of outer states in addition to the Coster-Kronig transition which decreased by $(1\text{-}P)^2$, P can be represented as:

$$P = \frac{q^2}{2\beta v_1^2}\left(1 - \frac{\beta}{4v_1^2}\right) \tag{4}$$

Where β=0.9 a dimensionless parameter $v_1 = 6.351\left[\frac{E_1(MeV)}{A_1(u)}\right]^{\frac{1}{2}}$ which is the velocity of the projectile in atomic units, v_0 = 2.19×10⁶m/s which is the velocity of an electron, the projectile atomic number Z_1 is replaced by its charge stat q. The formula used to calculate q is dependent of state. If target is a solid-state as in our case, q is given a

$$q_{equilibrme\ charge} = z_1 \frac{12x+x^4}{\frac{0.07}{x}+6+0.3x^{0.5}+10.3x+x^4} \tag{5}$$

$$x = \left(\frac{v_1}{v_0} z_1^{-0.52} \frac{Z_2^{0.019z_1^{-0.52}}}{1.68}\right)^{1+\frac{1.8}{z_1}} \tag{6}$$

If the probability in equation 4 is more than 1, the maximum value is taken as the probability. For example, if P = 1.9, the value of the probability to be used is 1 [50].

The single vacancy fluorescence yields ω_i^0 are corrected for simultaneous ionization in outer subshells as:

$$\omega_i = \omega_i^0[1 - P(1 - \omega_i^0)]^{-1} \tag{7}$$

While the Coster-Kronig yields f_{ij} for the multiple ionization are corrected by:

$$f_{ij} = f_{ij}^0(1 - P)^2 \tag{8}$$

The fractional rates S_{ij} remain unchanged since partial and total non- radiative widths are narrowed by identical factors.

Binding Energy, X-ray Energies and Intensity Ratios of Heavy Ion X-ray Production Cross Section

When a target atom undergoes multiple ionization, a reduction in the nuclear charge screening occurs. This phenomenon, in turn, leads to an increase in the binding energy of the remaining electrons in the atom. For example, in the case of L X-ray emission, when a target atom undergoes multiple ionization due to a projectile collision, several M vacancies will be present in addition to the single L vacancy. These M vacancies act as spectator vacancies during the L X-ray emission, meaning they remain unfilled until the L vacancy is radiatively filled. Since the binding energies of inner shells shift more significantly compared to outer shells, the difference in binding energies between two specific levels widens, resulting in a consequent increase in the energy of the emitted L X-ray.

The magnitude of the energy shift in the emitted X-rays is proportional to the increase in M vacancies. As a result, multiple ionized atoms emit X-rays that are shifted and broadened compared to the X-ray energies of singly ionized atoms (Figure 2). These emitted X-ray energies reflect the actual vacancy configuration during the emission process. This shift in the peak (centroid) of the L X-ray line, caused by heavy ion bombardment of the target material, is termed as "energy shift". The magnitude of this shift depends on two factors [55]: (i) the degree of multiple ionizations present in the target material, and (ii) the specific satellite. In addition to the L vacancies, the number of M to O vacancies can also be accessed during L X-ray emission. Multiple-ionization probabilities can be estimated using X-ray energy shifts and intensity ratios [1,4,6,7,48,56-61].

The Bissinger group [59], investigated the effects of multiple ionization on L X-ray emission by bombarding Au with 12-15 MeV oxygen ions. They observed a shift in the L-shell X-ray lines towards higher energy compared to the case with a single-hole vacancy. Similar observations of L X-ray energy shifts were reported by Pajek et al. [6] when bombarding Au, Bi, Th, and U with oxygen. Uchai et al. [61] studied the L X-ray energy shifts of different L X-ray components in various high Z elements bombarded with Ag ions. Bogdanović and co-workers [1], explored the degree of multiple ionization by analyzing X-ray line energy shifts and intensity ratios. They used C ion bombardment and compared the results with those obtained using proton bombardment. Verma et al. [58], measured energy shifts and intensity ratios

induced by N, Si, and Ti projectiles with various bombarding energies to examine the degree of multiple ionization in various targets.

In our previous work [4], we studied the X-ray production cross-sections (XPRSCs) of Y, Gd, and Bi due to carbon ion bombardment in the energy range of 2-12 MeV. We observed an energy shift in the X-rays towards higher energy. Additionally, we used the relative line intensities of the L X-ray lines to determine the degree of multiple ionization. We found that the energy shift depends on the atomic number of the bombarding ions, with ions having higher atomic numbers causing a greater energy shift compared to those with lower atomic numbers.

Experimental Procedures

The experimental procedures by the authors followed the standard practices for heavy ion-induced X-ray production cross-section measurements. For detailed experimental procedures, check all the papers review in this work [3,4,7,27,38,46,62,63]. Below is an overview of the experimental procedures used by the authors:

1. Experimental Setup:

The experiments used ion accelerators such as tandem accelerator, Van de Graaf. These accelerators are capable of producing heavy ion beams in the energy range of interest (typically MeV range) were used. The backscattered ion spectrum and the X-ray spectrum were measured using a variety of detectors, such as the HPGe, Si (Li), SDD, and PIPS detector.

2. Target Preparation and Characterization:

- Various techniques including, sputtering, electron beam deposition, magnetron was employed to prepare the target films.
- For the target thickness, techniques like RBS were utilized.

3. Charge Collection and Current Monitoring:

- The total incident ion charge was measured using Faraday cups (insertion or transmission type) or charge integrators.

4. Data Acquisition and Analysis:

- X-ray and backscattered particle spectra were simultaneous measured.
- The X-ray production cross-sections were calculated using formulas that essentially include normalizing the X-ray yields to the backscattered particle yields, detector solid angles, efficiency, and target parameters (thickness, composition).

5. Corrections and Considerations:

- Some of the papers carried out some corrections like the multiple ionization effect correction, energy loss correction.

6. Error Analysis and Uncertainty Estimation:

- Various sources of uncertainty were identified and quantified, such as target thickness, charge collection, detector efficiency calibration, and adjustments for energy loss, among other things.

Overall, the experimental methods detailed in the papers adhered to accepted standards for measuring the X-ray production cross-sections by heavy ions.

Comparison between Experimental Data and Theoretical Predictions

Several theoretical models, both quantum-mechanical and classical, have been developed to describe the phenomenon of atomic inner shell ionization caused by heavy ion collisions. These models aim to elucidate the various mechanisms, both simple and complex, involved in such collisions, offering insights into the microscopic and macroscopic dynamics of the interaction.

These theories categorized the colliding systems (the projectile and the target) according to the parameters Z_1/Z_2 and v_1/v_{2S}, where Z_1 and Z_2 are the atomic numbers of the projectile and the target, respectively, v_1 is the ion velocity and v_{2S} is the velocity of the electron in the inner shell of the target atom [29]. As described in section 2.0, inner-shell vacancies in the collision system can arise from either direct ionization (DI) or electron capture (EC) by the charged ion [2,4,29].

With this in mind, in this review the Plane Wave Born Approximate (PWBA) theory [65], Energy Loss Coulomb Deflection Perturbation Stationary State Relativistic (ECPSSR) theory [66-68], Energy loss (E) and Coulomb Deflection (C) Separate-United Atom ECUSAR) approximations [69], Semi classical approximation (SCA) [70] and First Born Approximations (FBA) together with their associated variants have been considered. Table 1 summaries the literatures used in this review from 2000 to 2023. A survey of L-shell X-ray production measurements for C and O ions from 1994 to 2005 has been summarized by Mehta et al. 2005 [32].

Comparison with Experimental Data and Plane Wave Born Approximation (PWBA) Predictions

Plane Wave Born Approximation (PWBA) [65] is based on perturbation theory to a transition from an initial state to a final state in which the First-Born approximation (FBA) is used to describe the interaction between the projectile ion and

Table 1: The summary of X-ray production cross sections induced by carbon ions.

Targets	Projectiles	Energy range (MeV)	X-ray measurements	Theoretical predictions	Reference (Year)
Re, Pt, and Au	^{12}C	4–8	L_α, L_β, L_γ, $L_{\gamma1}$, $L_{\gamma23}$, $L_{\gamma44}$	PWBA, ECPPSR, ECUSAR + SA, ECUSAR + IS	Lapicki el al. [50]
La, Ce, Nd and Sm	^{12}C	35–60	Total L-shell	FBA, ECPSSR	Mehta el al. [32]
Ce, Nd and Lu	^{12}C	4–10	L_ℓ, L_α, L_β, L_γ, $L_{\gamma15}$ $L_{\gamma23}$, $L_{\gamma44}$	PWBA, ECPPSR, ECUSAR + SA, ECUSAR + IS	Lapicki et al. [73]
Pt	^{12}C	0.4-5	L_α, L_β, L_γ	SCA-SA, SCA-UA, ECPSSR and ECPSSR-VC.	Gugiu et al. [3]
Ti, Fe Zn, Nb, Ru and Ta	^{12}C	3-12	L_α	ECPSSR-UA	Prieto et al. [40]
Ru and Ta	^{12}C	2.4-12	L_α, total L-shell	ECPSSR-UA and ECPSSR-EC	Msimanga et al. [50]
Ag and Au	^{12}C	2-5	L_α, L_β, L_γ, L_ℓ and total L-shell	PWBA, ECPSSR and ECUSAR	Silhadi et al. [64]
V and Zr	^{12}C	2-12	Total L-shell	PWBA and ECPSSR	Masekane et al. [7]
Sm and Yb	^{12}C	2-5	L_α, L_β, L_γ, L_ℓ and total L-shell	PWBA, ECUSAR and ECUSAR+MI	Silhadi et al. [38]
Gd, Bi and Y	^{12}C	2-12	Total L-shell	ECPSSR +UA, ECPSSR+EC	Ejeh et al. [4]
Zr, Nb, Mo, Ag, Cd, In, Sn, Sb, Ta, W, Pb, Bi	^{12}C	9.6–19.2	Total L-shell	ECPSSR and PWBA	Gorlachev et al. [50]

the target. The nature of the projectile ion, before and after collision, is described by plane wave functions [71] based on the condition:

$$Z_1 v_0 \ll v_1 \ll v_{2s} \tag{9}$$

where Z_1 is the atomic number of the incident ion, v_1 and v_{2s} are the velocities of the incident particle and orbital electron, respectively, and v_o is the Bohr velocity.

In the PWBA model, the differential cross section of the collision system is given as [85]:

$$\frac{d\sigma}{d\Omega} = \frac{k_f}{k_i}\left(\frac{2\mu}{4\pi\hbar}\right)^2 |< \psi_i |V| \psi_f >|^2 \tag{10}$$

where $<\psi i |V|>$ is the transition matrix element, ψi, Vi and ψf are the initial and the final wave vectors of the projectile-orbital electron system.

For asymmetrical collision, $Z_1 \ll Z_2$ and $v_1 \gg v_2$, and it is assumed that [72]:

i) The interaction between the incident ion and the target electron is very weak.

ii) The target electron appears "frozen" during collision because the response time of the electrons is long compared to the interaction time.

iii) The projectile acts as a point charge and its electronic structure has a negligible effect on the interaction.

The atomic cross section is represented in the expression in equation (11).

$$\sigma_i^{PWBA}(\sigma_{0K}) f_K(\eta_K, \vartheta_K), \tag{11}$$

with,

$$\sigma_{0K} = 8\pi a_0^2 \frac{z_1^2}{z_{eff}^4}$$

where Z_{eff} = (Z-c) is the effective charge of the atomic shell, c = 0.3 for the K and L_1 shells and c = 4:15 for L_2 and L_3 shells and

$$\eta_K = \frac{m_{0E}}{MR_h Z_{eff}^2} = \frac{1}{Z_{eff}^2}\left(\frac{e^2}{h\nu}\right)^2, \tag{11a}$$

$$f_K(\eta_K, \vartheta_K) = \int_{w_{min}}^{w_{max}} dw \int_{Q_{min}}^{Q_{max}} |(Q)|^2 \frac{dQ}{Q^2} x_i\left(\frac{\rightarrow}{r_2}\right), x_f\left(\frac{\rightarrow}{r_2}\right) \tag{11b}$$

where $F(q) = \int x_f^*\left(\frac{\rightarrow}{r_2}\right) e^{iq.r} x_i\left(\frac{\rightarrow}{r_2}\right) d_{\frac{\rightarrow}{r_2}}$, $x_i\left(\frac{\rightarrow}{r_2}\right), x_f\left(\frac{\rightarrow}{r_2}\right)$, are non-relativistic wave functions of atomic electrons and $x_f^*\left(\frac{\rightarrow}{r_2}\right) et\ x_f^*\left(\frac{\rightarrow}{r_2}\right)$ are the complex conjugates of the wave functions, $Q = (a_s, q_s)^2$, a_s, q_s are the radius of the atomic shell and transferred momentum relative to the atom shells, respectively.

Silhadi et al. (2019) [38], Masekane et al. (2020) [7], Silhadi et al. (2020) [64] and Gorlachev et al. 2021 [27] measured the L shell X-ray production cross sections of different elements induced by carbon ions and compared their experimental data with the theoretical prediction of the PWBA.

Silhadi et al. [38,64] measured the individual (L_α, L_β, L_γ, L_ℓ) and total L-shell X-ray production cross sections for silver (Ag) and gold (Au) induced by carbon ions within an energy range of 2.8-5 MeV. Likewise, they measured similar cross sections for samarium (Sm) and ytterbium (Yb) using carbon ions in the 2-5 MeV range.

Ejeh E, et al., J Biotechnol Biomed 2024
DOI:10.26502/jbb.2642-91280170

Similarly, Masekane et al. (2020) measured the L-shell X-ray production cross sections in zirconium (Zr) and tin (Sn) due to carbon ion beams with an energy range of 4 MeV – 12 MeV.Gorlachev and co-workers [27] investigated the L-shell X-ray production cross sections in zinc (Zn), niobium (Nb), molybdenum (Mo), silver (Ag), cadmium (Cd), indium (In), tin (Sn), antimony (Sb), tantalum (Ta), tungsten (W), lead (Pb), and bismuth (Bi). The energy range of carbon ions used in their study was 9.6 MeV to 19.2 MeV.

All the aforementioned studies, encompassing silver (Ag), gold (Au), samarium (Sm), ytterbium (Yb), zirconium (Zr), tin (Sn), zinc (Zn), niobium (Nb), molybdenum (Mo), cadmium (Cd), indium (In), antimony (Sb), tantalum (Ta), tungsten (W), lead (Pb), and bismuth (Bi), reported that the PWBA consistently overestimated both the individual and total L-shell X-ray production cross sections.

Note that the individual L_{α}, L_{β}, L_{γ}, $L_{\gamma 1}$, $L_{\gamma 23}$, $L_{\gamma 44}$ X-ray production cross sections measured by Lapicki et al. [50] and Lapicki et al. [73] were used mainly for the extraction of ionization cross sections and are therefore not comprehensively discussed in this work

There is good agreement between PWBA and experiment for light projectiles at high velocities but when heavy-ion projectiles are used, the perturbation corrections become impossible especially under slow collision conditions. These complications arise as a result of modification of the binding energy of the electrons of the target in presence of the projectile ion, Coulomb deflection of the projectile due to the target nucleus and enhanced cross-section for electron transfer from the bound state of the target atom to the bound state of the projectile ion. The ionization cross section therefore reduces as a result of shallow interaction between the ions and the targets [38].

Comparison with Experimental Data and Energy Coulomb Perturbed Stationary State Relativistic (ECPSSR) Prediction and its Variants

Building upon the Plane-Wave Born Approximation (PWBA), Brandt and Lapicki [66] introduced the Energy Loss Coulomb Perturbation Stationary State Relativistic (ECPSSR) model. This refined model incorporates corrections for Coulomb repulsion, projectile energy loss, relativistic effects and binding polarization effects. Utilizing the ECPSSR model, the L-shell ionization cross section can be expressed as:

$$\sigma_{Li}^{ECPSSR} = C_{BLi}^{E}\left(d_{qos}^{B}\xi_{Li}\right)\sigma_{Li}^{pWBA}\ \frac{m_{Li}^{R}\left(\frac{\xi_{Li}}{\zeta_{Li}}\right)\eta_{Li}}{\zeta_{Li}\,\theta_{Li}}, \zeta_{Li}\theta_{Li}\ , \qquad (12)$$

Where, C_{BLi}^{E} is the Coulombian deflection term, which dictates that there is a probability that the projectile can be deviated in the field of the target nucleus, ζ_L is a correction for the binding energy and polarization effects and $m_L^R\left(\frac{\xi_{Li}}{\zeta_{Li}}\right)$ is the relativistic effect correction.

Mehta et al. [32] measured the cross sections of La, Ce, Nd, and Sm at 35-60 MeV and found better agreement with the ECPSSR model for higher Z elements (Nd and Sm) than for lower Z elements (La and Ce).

Gugiu et al. [3] measured the individual L_{α}, L_{β} and L^{γ} lines of Pt at 6-54 MeV and found that the ECPSSR model provided the best description, with Lα lines showing the best agreement. However, they observed an "overbinding behavior" at low energies that increased with projectile atomic number [74].

Silhadi et al. [38] measured the individual and total L lines of Ag and Au at 2-5 MeV and reported good agreement with the ECPSSR model at high energy but observed a disparity at low energy, consistent with the findings of Bhattacharya et al. [75] for Au at higher energy and Sarkadi et al. [76] at lower carbon energy.

The total L shell X-ray production cross sections for Zr and Sn metal oxide films induced by 4 MeV to 12 MeV ^{12}C were experimentally measured and compared with the ECPSSR model and ECPSSR+EC by Masekane et al. [7]. Both models exhibited similar trends, with agreement with the experimental data improving as the projectile energy increased. Their result show the same trend as the work of Mehta et al. [62].

In our previous study [4], we investigated the total L-shell X-ray production cross section measurements for the elements Y, Gd, and Bi. The measurements were conducted using 4 MeV– 12 MeV ^{12}C projectile ions. The experimental data were compared with theoretical calculations based on the ECPSSR, along with its variants ECPSSR+EC and ECPSSR+UA. Developed by Sarkadi and Mukoyama [77], the ECPSSR+UA model refines the original ECPSSR by improving its description of heavy-ion collisions. This refinement is achieved through a correction to the binding energies of target electrons, accounting for the influence of the incident ion. Unlike ECPSSR's Perturbed Stationary State (PSS) treatment, the ECPSSR+UA model employs a combined "united (U) and separated (S) atom (A)" formula.

In our study, the experimental data for Y, Gd and B show the same trend as the theoretical prediction. The Y and G data generally agree with existing trends reported by Mehta et al. [62] and Lugo-Licon [8]. It was noted that While the ECPSSR theory generally aligns with existing literature data, our data at lower energies is better described by the ECPSSR + EC modification**.** However, for Bi, no data on carbon-bismuth interaction was found in the literature for this energy range. All theoretical predictions overestimate our data by a factor of roughly two, despite their agreement with each other. At higher energies (approaching 1.0 MeV/u), both data sets show good agreement with the basic ECPSSR model

Ejeh E, et al., J Biotechnol Biomed 2024
DOI:10.26502/jbb.2642-91280170

for direct ionization, suggesting the additional modifications become less significant. We concluded that for this ion-target pair at these beam energies, the consistency among the three theoretical calculations suggests that the UA and EC modifications beyond direct ionization have negligible influence.

Gorlachev et al. [27] measured total L-shell X-ray production cross sections for Zr, Nb, Mo, Ag, Cd, In, Sn, Sb, Ta, W, Pb, and Bi induced by 9.6–19.2 MeV ^{12}C ions. Comparing their results with the ECPSSR model revealed good agreement. Observed discrepancies were attributed to the inherent limitations of theoretical models and the existence of specific applicability domains for different theoretical predictions.

Msimanga et al. [46] focused on X-ray production in thin films of ruthenium and tantalum, bombarded with carbon ions (^{12}C) at energies ranging from 0.2 to 1.0 MeV/u. Comparing their results with the ECPSSR+UA theory, they specifically analyzed the Lα line for tantalum (Ta) and compared it to various models: ECPSSR with UA and EC variants, as well as the findings of Prieto et al. [40]. They reported a fair agreement between their work and that of Prieto and co-workers. Analysing the tantalum data, the researchers found that the ECPSSR+UA model better matched the experimental results when $Z_{ion}/Z_{target} \ll 1.0$, improving with higher beam energies. Interestingly, electron capture (EC) had no significant effect on this specific collision (^{12}C on Ta), but it became crucial in the case of ^{12}C on ruthenium, where the ECPSSR+EC model outperformed ECPSSR+UA. These findings highlight that the contribution of EC heavily depends on the unique characteristics of each collision system, as demonstrated by the varying roles it played in the experiments conducted by Msimanga et al [46].

Comparison with Experimental Data and Energy Coulomb United Separate Atom Relativistic (ECUSAR) Prediction and its Variants

To improve predictions of ion-atom interactions, Lapicki [69] developed the ECUSAR theory, refining the ECPSSR model by adjusting target electron binding energies. This is achieved by replacing the ECPSSR's "perturbed stationary state" (PSS) with a combined "united atom" (UA) and "separated atom" (SA) approach, as expressed in the following equation:

$$\zeta_L^{USA} = \begin{cases} \zeta_L^{UA}, when\ \zeta_L^{UA} \leq \zeta_L \quad for\ slow\ collision\ regime \\ \quad\quad and \\ \zeta_L\,\zeta_L^{UA}, for\ intermediate\ to\ fast\ collision\ regime \end{cases} \quad (13)$$

ζ_L replaces the one which was derived in the separated atom PSS in ECPSSR model.

Where,

$$\zeta_L^{USA} = \left(\frac{1+\frac{2z_1}{Z_{2s}}}{\theta_s}\right)^2 \theta_s^{UA}$$

The ECUSAR model for L shell ionization cross section is given as:

Where,

$$\sigma_L^{ECUSAR} = C_{BL_i}^E(d_{qos}^B\ \zeta_L)\sigma_L^{PWBA}\left(m_{Li}^R \frac{\left(\frac{\xi_{Li}}{\zeta_{Li}^{USA}}\right)\eta_{Li}}{\left(\zeta_{Li}^{USA}\right)^2},\ \zeta_{Li}^{USA}\theta_{Li}\right) \quad (14)$$

C_{BL}^E is the Colombian deviation term giving the probability that the projectile can be deflected in the field of the nucleus of the target atom [69]. $m_{Li}^R(\frac{\xi_L}{\zeta_L})$ is the relativistic mass correction,and ζ_L is a correction of the binding energy and the polarization effects [69], the dimensionless variable θ_{Li} are the reduced binding energy [65].

Silhadi et al. [38] investigated the individual and total L-shell X-ray production cross sections (XRPCS) for Au and Ag bombarded with 2.8-5.0 MeV ^{12}C ions. They compared their results with the ECUSAR model and observed a good agreement between the model and individual L-shell XRPCS across all projectile energies. The total L-shell XRPCS for both Au and Ag also show cased good agreement with the model at lower incident energies

Comparing their data with those found in the literature, they observed trends in the data which agreed with those reported by Sarkadi et al. [76] at lower energies and Bhattacharya et al. [75] at higher energies. However, a significant discrepancy was found with the data of Mehta et al. [62]. They reported that multiple effect correction was negligible.

Silhadi et al. [64], measured the individual and total L-shell X-ray production cross sections (XRPCS) for Sm and Yb bombarded with 2.0-5.0 MeV ^{12}C ions, comparing their results to the ECUSAR model. Good agreement was observed between the experimental data and the model for the individual L-shell lines of both Sm and Yb. Their data generally agreed with Lugo-Licona et al. [8] at lower energies (6-10 MeV), except for the L_ℓ line. This deviation is attributed to the inherent anisotropic nature of L_ℓ radiation emission. A similar observation was made for the L_ℓ XRPCS in Yb data when compared with Bogdanovic et al. [1]. Both elements exhibited good agreement between their total L-shell XRPCS and the ECUSAR model. Notably, incorporating multiple ionization (MI) further improved the model's agreement with the Sm data, but no such improvement was observed for Yb.

Comparison with Experimental Data and Semi-Classical Approximation (SCA) Prediction and its Variants

Bang and Hansteen's semi-classical approximation (SCA) [78] investigates the deflection and deceleration of light ions colliding with atoms due to Coulomb excitation. It employs a hybrid approach, treating the projectile's motion classically and the inner-shell electron's transition to the continuum quantum mechanically [79]. This model excels

Ejeh E, et al., J Biotechnol Biomed 2024
DOI:10.26502/jbb.2642-91280170

when projectile energies are significantly lower than target atom binding energies. In such scenarios, the projectile's deflection in the target's Coulomb field is calculated using impact parameters. Crucially, for the SCA to accurately describe ionization classically, the moving ion's de-Broglie wavelength must be much smaller than the distance of closest approach [79] i.e.,

$$\frac{2d}{\lambda} = \frac{2Z_1 Z_2 e^2}{h v_1^2} \gg 1 \quad (15)$$

The above ratio is termed coulomb parameter, λ is the de-Broglie wavelength, d is the half distance of the closest approach in a head-on collision and it is given by:

$$d = \frac{Z_1 Z_2 e^2}{M_1 v_2^2} \quad (16)$$

The Semi-classical Approximation (SCA) sheds light on the collision process as a function of the impact parameter. Derived from the fundamental principles of quantum mechanics (specifically, first-order time-dependent perturbation theory), in a relatively straightforward approach. The correction such as the relativistic wave functions [67,80,81], the hyperbolic trajectory of the projectile [82,83] and the corrections for the binding-polarization [66,80] on the semi-classical approximation [68,84] approaches for direct ionization have helped improve agreement between the theory and experiment. The application of the hyperbolic trajectories in the SCA predictions for coulomb excitation has been proven experimentally to give good agreement with experimental data for lower energies. In the SCA model [85], the electron binding effect is treated in both the united-atom (UA) and separated-atom (SA) limits.

Gugiu et al. [3] explored the L-shell X-ray production cross-section (XRPCS) of Platinum (Pt) using 0.5-4 MeV/u carbon ions. They compared their findings with the semi-classical approximation (SCA) and its variants, specifically SCA-UA and SCA-SA, focusing on individual L lines (L_α, L_β, L_γ, L_l). While SCA-UA showed good agreement with the data at lower energies, it diverged at higher energies. Conversely, SCA-SA consistently overestimated the experimental results. Gugiu et al. attributed the observed behavior of SCA-UA at higher energies to the breakdown of the adiabatic conditions assumed by the model.

Comparison with Experimental Data and First-Born Approximation (FBA) Prediction

The first order born approximation captures the sum of cross sections for direct ionization and electron capture [86,87]. The L_i subshell ionization cross section can be expressed as [86]:

$$L_i = 8\pi Z^2 a_0^2 Z_L^{-4} \eta_L^{-1} f_{Li} \quad (17)$$

Where:

$$f_{Li} = \int_{\theta_{Li}/4}^{\infty} I_{Li}(\eta_L, W) dW, (i = 1,2,3) \quad (18)$$

The total L shell ionization cross sections σ_L and the total L XRPCS σ_{LX} are written as:

$$\sigma_L = \sigma_{L1} + \sigma_{L2} + \sigma_{L3} + \sigma_{L1} = 8\pi Z^2 a_0^2 Z_L^{-4} \eta_L^{-1} f_L \quad (19)$$

$$\sigma_{LX} = v_1\sigma_{L1} + v_2\sigma_{L2} + v_3\sigma_{L3} = \overline{\omega}_L \sigma_L \quad (20)$$

$$f_L = f_{L1} + f_{L2} + f_{L3}$$

$$v_1 = \omega_1 + f_{12}\omega_2 + (f_{13} + f_{12} f_{23})\omega_L$$

$$v_2 = \omega_1 + f_{12}\omega_3$$

$$v_2 = \omega_3$$

The fluorescence yield for the L_i-subshell is ω_3 (i = 1,2,3), and $\overline{\omega}_L$ is an average flourescence yield for the entire L-shell. The quantities f_{ij} $((ij = 1,2,3)$

Mehta et al. 2005 [32] measured L-shell X-ray production cross-sections (XRPCS) for La, Ce, Nd, and Sm under bombardment by 35-50 MeV ^{12}C ions, comparing their results with predictions from the First-Born Approximation (FBA). They found good agreement with FBA for the heavier elements La and Ce (higher Z values), but significant discrepancies for Nd and Sm (lower Z values). The observed difference between their experimental data and the theoretical predictions was attributed to Multiple Ionization (MI), which was not considered in their analysis. Additionally, they identified shortcomings in the efficiency of the detector used for the measurements.

This review study covers a wide range of elements, including Ag, Au, Sm, Yb, Zr, Sn, Zn, Nb, Mo, Cd, In, Sb, Ta, W, Pb, and Bi. The energy range of carbon ions used varies from study to study, with some focusing on lower energies (2-5 MeV) and others on higher energies (up to 60 MeV).

The PWBA agrees well with experimental data for light projectiles at high velocities but for heavy- ion projectiles at lower velocities. The result consistently overestimated experimental data across various collision systems, indicating limitations in predicting XRPCS, especially for heavy-ion projectiles and slow collision conditions and hence perturbation corrections become necessary owing to factors like electron binding energy modifications, Coulomb deflection, and electron transfer.

Comparing the ECPSSR model with experimental data show mixed results, with better agreement observed for higher Z elements, particularly at higher energies but tend to overestimate the cross sections at lower energy, these observed discrepancies, especially at low energies, indicate limitations in the model's accuracy, particularly in describing overbinding behavior of the electrons to the atom, and it's not capturing the unique features of certain collision setups as aspected. The various variants like ECPSSR+UA and

Ejeh E, et al., J Biotechnol Biomed 2024
DOI:10.26502/jbb.2642-91280170

ECPSSR+EC exhibit varying degrees of success depending on the collision system and energy range.

ECUSAR improves the ECPSSR by modifying target electron binding energies and utilizing both united and separated atom approaches. When compared with experimental data, there was generally good agreement, especially when it came to lower incident energies, even better than the ECPSSR model for certain ion-target combination. This because it refines the binding energy calculations compared to ECPSSR, potentially leading to a more accurate description of electron projectile interactions at lower velocities. Incorporating multiple ionization (MI) further improved the agreement between the ECUSAR model and the experimental data at lower energies for some elements like Sm. However, as long as this review is concerned, more data at lower energies for ECUSAR is needed for a definitive conclusion.

SCA model showed good agreement with the experimental data at lower energy just like the ECUSAR model but diverge at higher energies, indicating a break down od adiabatic conditions. The SCA variants like SCA-UA and SCA-SA exhibited varying degrees of accuracy with SCA- UA performing better at lower energies but still maintaining the limitations at higher energies.

The FBA generally demonstrated better agreement with experimental data for heavier elements (higher Z), while encountering challenges with lighter elements. This difficulty arises from its omission of multiple ionization effects. This contrast with PWBA model which exhibited good agreement with experimental results for light elements when ion velocity is high.

Generally, the inclusion of corrections like MI, EC, UA and atomic parameter seemed to improve the agreement between theory and experiment, but their contributions vary depending on the specific ion-target combination and energy range. We can therefore say that, different theoretical models perform better in different energy regimes and for different ion-target combinations, indicating the need for more comprehensive and accurate models that can account for various effects across a wide range of conditions. While there are some consistencies in the overall trends,

there are also discrepancies between different experimental studies and theoretical models, which can be attributed to factors such as detector efficiencies, specific experimental conditions, and the inherent limitations of the theoretical models themselves. For achieving accurate and consist alignment between theoretical predictions and experimental observations, it's essential to take all these factors into account.

Conclusion

The recent interest in the use of heavy ions for PIXE measurements, which is usually done with light ions, prodded the compilation of X-ray production cross sections due to carbon ions. We discovered that carbon, among other heavy ions, is the most frequently used ion for the inducement of ionization cross sections. While there's a general trend of overestimation by theoretical models compared to experimental data, the specific agreement and discrepancies vary depending on the elements studied, the energy range of the projectiles, and the specific theoretical models used. With the data examined in this review, carbon ions can well be predicted using ECPSSR and ECUSAR theories and can also be used for heavy ion PIXE applications because in most cases, as examined here, the experimental data generally align well with theoretical predictions, ranging from very good to at least satisfactory agreement. However, there's room for improvement in fine- tuning certain aspects of these theories, particularly at lower projectile energies. The number of XRPCS by carbon ions as reviewed in this work shows that, carbon ion XRPCS is still limited. Therefore, there is a need for continuous and conscious X-ray production cross section measurements due to carbon ions by PIXE groups to cover up the existing energy gaps of various ion-atom collision systems, even though it will be a herculean task to measure the X-ray production cross sections for all ion-atom combinations conceivable. It will be important that more reviews on other heavy ions XRPSC be investigated to ascertain the progress global PIXE practitioners have attained in increasing the existing heavy ion XRPCS global database. Furthermore, it was clearly observed that different collision systems involve varying mechanisms and interactions between particles. The specific elements involved in the collision and the energy levels at play significantly influence the dynamics of the interaction. This, in turn, affects the accuracy of the chosen model.

References

1. Bogdanović I, Fazinić S, Jakšić M, et al. '*L*-shell ionization of selected medium-*Z* elements by 0.22–0.83-MeV u^{-1} carbon ions. Physical Review A 56 (1997): 2860-2867.

2. Kumar S, Singh U, Oswal M, et al. L shell x ray production in high-Z elements using 4–6 MeV/u fluorine ions. Nuclear Instruments and Methods in Physics Research, Section B: Beam Interactions with Materials and Atoms 395 (2017): 39-51.

3. Gugiu MM, Ciortea C, Dumitriu D, et al. Pt L X-rays production cross sections by ^{12}C, ^{16}O, ^{32}S and ^{48}Ti ion-beams in the MeV/u energy range. Presented at the : 10th International Balkan Workshop on Applied Physics, Romanian Journal of Physics Jan (2011): 71-79.

4. Ejeh EO, Hlatshwayo TT, Madhuku M, et al. Measurement of L-shell X-ray production cross sections in 89Y, 158Gd and 209Bi due to 0.3 MeV/u – 1.0 MeV/u 12C ions. Applied Radiation and Isotopes 177 (2021): 109930.

5. Hubbell JH, Trehan PN, Singh N, et al. A Review, Bibliography, and Tabulation of K, L, and Higher Atomic Shell X-Ray Fluorescence Yields. Journal of Physical and Chemical Reference Data 339 (1994).

6. Pajek M, Banaś D, Braziewicz J, et al. L X-ray emission induced by heavy ions', Nuclear Instruments and Methods in Physics Research, Section B: Beam Interactions with Materials and Atoms 363 (2015): 19-23

7. Masekane MC, Moloi SJ, Madhuku M, et al. Measurement of ^{12}Cq+ and ^{35}Clq+ ion induced X-ray production cross sections in V, Zr and Sn metal oxide films at 0.1 MeV/u - 1.0 MeV/u energies. Radiation Physics and Chemistry 176 (2020): 109083.

8. Lugo-Licona M, Miranda J, Romo-Kröger CM. L-shell X-ray production cross section measured by heavy ion impact on selected rare earth elements. Journal of Radioanalytical and Nuclear Chemistry 262 (2004): 391-401.

9. Govil IM. Proton induced X-ray emission - A tool for non-destructive trace element analysis. Current Science 80 (2001): 1542-1549.

10. Hajivaliei M, Puri S, Garg ML, et al. K and L X-ray production cross sections and intensity ratios of rare-earth elements for proton impact in the energy range 20-25 MeV. Nuclear Instruments and Methods in Physics Research, Section B: Beam Interactions with Materials and Atoms 160 (2000): 203-215.

11. Chen JR. An application of PIXE in medicine: Legionnaires' Disease. Nuclear Instruments and Methods 181 (1981): 337-343.

12. Alessandro Z, Andrés RC. Ion beam analysis: New trends and challenges. Nucl Instrum Methods Phys Res B 331 (2014): 48-54.

13. Kasahara M, H€oller R, Tohno S, et al. Application of PIXE technique to studies on global warming/cooling effect of atmospheric aerosols. Nucl Instrum Methods Phys Res B 189 (2002): 204-208.

14. Schmelmer O, Dollinger G, Datzmann G, et al. Particle-induced X-ray emission using high energy ions with respect to microprobe application. Nuclear Instruments and Methods in Physics Research Section B: Beam Interactions with Materials and Atoms 179 (2001): 469-479.

15. Johansson S, Campbell J, Malmqvist K. Particle-Induced X-Ray Emission Spectrometry (PIXE). Wiley-interscience (1995).

16. Deghfel B, Kahoul A, Abdellatif A, et al. Proton induced K-shell ionization cross sections for a wide range of elements ($4 \leq Z \leq 92$) within ECPSSR theory and updated experimental data. Journal of Radiation Research and Applied Sciences (2014).

17. Miranda J, Lapicki G. Experimental cross sections for L-shell X-ray production ionisation by protons. At. Data Nucl Data Tables 100 (2014): 651-780.

18. Lapicki G, Lapicki RM. Multiple outer-shell ionization effect in inner-shell x-ray production by light ions. Physical Review A (1986).

19. Braziewiczt E, Braziewicz J, Czyzewski T, et al. L-subshell ionization of rare earth elements by light ion bombardment. Journal of Physics B: Atomic, Molecular and Optical Physics J Phys E: At Mol Opt Phys 7 (1991): 1669-1682.

20. Crawford J, Cohen DD, Doherty G, et al. Calculated K, L, and M shell X- ray line intensities for light ion impact on selected targets from Z= 6 to 100. Institute for Environmental Research Australian Nuclear Science and Technology Organisation (2011).

21. Jitschin W, Hippler R, Finck K, et al. L-subshell ionisation of Au by light-ion impact. Journal of Physics B: Atomic and Molecular Physics 16 (1983): 4405-4417.

22. Paul H. K-shell ionization due to light ions: The status of cross-sections', Nuclear Instruments and Methods in Physics Research Section B: Beam Interactions with Materials and Atoms 4 (1984): 211-217.

23. Vigilante M, Cuzzocrea P, Cesare ND, et al. Light- ion-induced Li ionization of $46 < Z < 60$ elements: First and Second-order corrections to PWBA (1990).

24. Paul H, Muhr J. Review of experimental cross sections for k-shell ionization by light ions. Physics Reports 135 (1986): 47-97.

25. Msimanga M, Pineda-Vargas CA, Madhuku M. K-shell X-ray production cross sections in Ti by 0.3-1.0 MeV/u^{12}C and ^{28}Si ions for heavy ion PIXE. Nuclear Instruments and Methods in Physics Research, Section B: Beam Interactions with Materials and Atoms 380 (2016): 90-93.

26. Ryan CG, Cousens DR, Sie SH, et al. Quantitative analysis of PIXE spectra in geoscience applications (1990).

27. Gorlachev I, Gluchshenko N, Ivanov I, et al. X-ray production cross sections induced by carbon ions', Nuclear Instruments and Methods in Physics Research, Section B: Beam Interactions with Materials and Atoms 499 (2021): 100-106.

28. Scafes AC, Ciortea C, Dumitriu DE, et al. K-shell ionization cross sections of Ti , Cr , Ni , Cu , and Zr in collisions with 16 O ions at Mev / u energies. Romanian Reports in Physics 66 (2014): 455- 471.

29. Batyrbekov E, Gluchshenko N, Gorlachev I, et al. X-ray production cross section for K-, L- and M-shell by 14 MeV and 19.6 MeV nitrogen. Nuclear Instruments and Methods in Physics Research, Section B: Beam Interactions with Materials and Atoms 330 (2014): 86-90.

30. Ozafrán MJ, Debray ME, Eusebi R, et al. K X-ray production induced by12C on several elements', Nuclear Instruments and Methods in Physics Research, Section B: Beam Interactions with Materials and Atoms (2003).

31. Ozafrán MJ, Vázquez ME, Romo ASMA, et al. Heavy ion induced X-ray emission work at the TANDAR laboratory in Buenos Aires', Nucl Instrum Methods Phys Res B 95 (1995): 1-3.

32. Mehta R, Puri NK, Kumar A, et al. L x-ray production in 57La, 58Ce, 60Nd and 62Sm by 35-60 MeV carbon and oxygen ions. Nuclear Instruments and Methods in Physics Research, Section B: Beam Interactions with Materials and Atoms 241 (2005): 1-4.

33. Kamada T, Tsujii H, Blakely EA, et al. Carbon ion radiotherapy in Japan: an assessment of 20 years of clinical experience. Lancet Oncology 16 (2015): e93-e100.

34. Amaldi U, Kraft G. Radiotherapy with beams of carbon ions', Reports on Progress in Physics 68 (2005): 1861.

35. Kamada T. Overview of clinical experiences on carbon ion radiotherapy at NIRS. Radiother Oncol 73 (2004): S41-S48.

36. Hu W, Li P, Hong Z, et al. Functional imaging-guided carbon ion irradiation with simultaneous integrated boost for localized prostate cancer: study protocol for a phase II randomized controlled clinical trial. Trials 23 (2022): 934.

37. Li Y, Li X, Yang J, et al. Flourish of Proton and Carbon Ion Radiotherapy in China. Front Oncol 12 (2022): 819905.

38. Silhadi H, Fazinic S, Haidra A, et al. L-shell X-ray production cross sections of Ag and Au induced by carbon ions between 2 MeV and 5 MeV. Nuclear Instruments and Methods in Physics Research, Section B: Beam Interactions with Materials and Atoms 459 (2019): 158-165.

39. Orlic I, Sow CH, Tang SM. Experimental L-Shell X-Ray Production and Ionization Cross Sections for Proton Impact. Atomic Data and Nuclear Data Tables 56 (1994): 159-210.

40. Prieto JE, Galán P, Zucchiatti A. Cross sections of X-ray production induced on Ti, Fe, Zn, Nb and Ta by O, Cl, Cu and Br ions with energies between 4 MeV and 40 MeV. Nuclear Instruments and Methods in Physics Research, Section B: Beam Interactions with Materials and Atoms 410 (2017): 102-107.

41. Kónya J, Nagy N. Nuclear and Radiochemistry, Second (2018).

42. Gudennavar SB, Badiger NM, Thontadarya SR, et al. K-shell fluorescence parameters of medium-Z elements. Radiation Physics and Chemistry 68 (2003): 721-726.

43. Anagnostopoulos DF. K fluorescence yields and level widths, in the presence of an l spectator hole. Journal of Physics B: Atomic, Molecular and Optical Physics 28 (1995): 47-53.

44. Deslattes RD, Kassler EG, Indelicato P, et al. X-ray transition energies: New approach to a comprehensive evaluation', Reviews of Modern Physics 75 (2003): 35-99.

45. Miranda J, Lucio OGD, Lugo-Licona MF. X-ray production induced by heavy ion impact: challenges and possible uses', REVISTA MEXICANA DE F´ISICA S53 (2007): 29-32.

46. Msimanga M, Pineda-Vargas CA, Madhuku M. L-shell X-ray production cross sections in metal oxide thin films due to ^{12}C, ^{16}O and ^{28}Si ion beams at MeV SIMS energies. Nuclear Instruments and Methods in Physics Research Section B: Beam Interactions with Materials and Atoms 440 (2019): 186-190.

47. Wolfli W. Heavy Ion Physics. In: Ceausescu V, Dorobantu IA (Eds.) Predeal International Summer School (Central Institute of Physics, Bucharest) (1976), pp: 43.

48. Berinde A, Ciortea C, Enulescu A, et al. On the L-M-N multiple ionisation in heavy elements. Journal of Physics B: Atomic and Molecular Physics 20 (1987): 15.

49. Miranda J, de-Lucio OG, Tellez EB, et al. Multiple ionization effects on total L-shell X-ray production cross sections by proton impact. Radiation Physics and Chemistry 69 (2004): 257-263.

50. Lapicki G, Murty GAVR, Raju GJN, et al. Effects of multiple ionization and intrashell coupling in L-subshell ionization by heavy ions. Physical Review A - Atomic, Molecular, and Optical Physics 70 (2004).

51. Benka O. The influence of multiple ionization upon fluorescence yield', Nuclear Instruments and Methods in Physics Research Section B: Beam Interactions with Materials and Atoms 4 (1984): 279-282.

52. Banaś D, Braziewicz J, Czarnota M, et al. Closing of Coster–Kronig transitions in multiply ionised gold atoms. Nucl Instrum Methods Phys Res B 205 (2003): 139-143.

53. Czarnota M, Banaś D, Braziewicz J, et al. X-ray study of M -shell ionization of heavy atoms by 8.0-35.2-MeV Oq+ ions: The role of the multiple-ionization effects', Physical Review A - Atomic, Molecular, and Optical Physics 79 (2009): 1-14.

54. Czarnota M, et al. X-ray study of M -shell ionization of heavy atoms by 8.0-35.2-MeV Oq+ ions: The role of the multiple-ionization effects', Physical Review A - Atomic, Molecular, and Optical Physics, 2009, doi: 10.1103/PhysRevA.79.032710.

55. Uchai W, Nestor Jr. CW, Raman S, et al. Energy shifts of l x-rays from 70 =s 2 4 90 elements due to multiple m vacancies. Atomic Data and Nuclear Data Tables 44 (1986): 201-214.

56. Kocbach L. On the Binding Effect on Inner Shell Ionization in Asymmetric Ion-Atom Collisions. Nuclear Instruments and Methods in Physics Research, Section B: Beam Interactions with Materials and Atoms 232 (B4): 248-261.

57. Pepper GH, Lear RD, Gray TJ, et al. L-shell x-ray production cross sections for O16 ions on Ce, Pr, Sm, Eu, Dy, and Ho: 0.50 to 2.25 MeV/amu. Physical Review A 12 (1975): 1237-1245.

58. Verma P, Braich JS, Mandal A, et al. Multiple Ionization Produced in Yb due to N, Si and Ti ion Impact. Physica Scripta 61 (2000): 335.

59. Nettles PH, Bissinger SMSG. X-ray production cross sections, intensity ratios, and centroid energy shifts of Ag K and I. and Au I. x rays produced by 160 beams of 12—50 MeV', Physical Principles of Electron Microscopy - An Introduction to TEM, SEM and AEM, 951–952. 10 (1974): 5–24.

60. Burkhalter PG, Knudson AR, NagelKnudson DJ. Ion-Excited Germanium g-Series X-Ray Spectra. Physical Review A 1 (1973): 105-112.

61. Uchai W, Nestor CW, Raman S, et al. Energy Shifts of L X-rays from 70 =s 2 4 90 elements due to multiple M vacancies', Atomic Data and Nuclear Data Tables 44 (1986): 201-214.

62. Mehta R, Sun HL, Marble DK, et al. L-shell X-ray production by 2-12 MeV carbon ions in fifteen selected elements from copper to lead.', Journal of Physics B: Atomic, Molecular and Optical Physics 28 (1995): 1187-1189.

63. Prieto JE, Zucchiatti A, Galán P, et al. Cross sections of X-ray production induced by C and Si ions with energies up to 1 MeV/u on Ti, Fe, Zn, Nb, Ru and Ta', Nuclear Instruments and Methods in Physics Research Section B: Beam Interactions with Materials and Atoms 406 (2017): 167-172.

64. Silhadi H, Ouziane S, Fazinic S, et al. L-shell x ray production cross sections of Sm and Yb induced by carbon ions between 2 MeV and 5 MeV. Nuclear Instruments and Methods in Physics Research, Section B: Beam Interactions with Materials and Atoms 478 (2020): 252-259.

65. Merzbacher E, Lewis HW. X-ray Production by Heavy Charged Particles, vol. 904, no. 1. Springer (1958).

66. Brandt W, Lapicki G. Energy-loss effect in inner-shell Coulomb ionization by heavy charged particles. PHYSICAL, REVIEW A 23 (1981): 1717.

67. Brandt W, Lapicki. Binding and Coulomb-deflection effects in L -shell Coulomb ionization by heavy charged particles. Low particle velocities. Physical Review A 10 (1974): 474-483.

68. Brandt W, Lapicki G. L-shell Coulomb ionization by heavy charged particles. Physical Review A 20 (1979): 465-480.

69. Lapicki G. The status of theoretical L-subshell ionization cross sections for protons. Nuclear Instruments and Methods in Physics Research, Section B: Beam Interactions with Materials and Atoms 189 (2002): 1-4.

70. Hansteen JM, Mosebekk OP. Atomic Coulomb excitation by heavy charged particles. Nuclear Physics, Section A 201 (1973): 541-560.

71. Ouziane S, Amokrane A, Zilabdi M. Experimental measurements of X-ray production cross-sections by protons of energies between 1 and 2.3 MeV and comparison with theoretical predictions of PWBA and ECPSSR models. Nuclear Instruments and Methods in Physics Research Section B: Beam Interactions with Materials and Atoms 161–163 (2000): 141-144.

72. Basbas G, Brandt W, Laubert R. Universal cross sections for k-shell ionization by heavy charged particles. I. Low particle velocities. Physical Review A 7 (1973): 983-1001.

73. Lapicki G. The status of theoretical K-shell ionization cross sections by protons', in X-Ray Spectrometry (2005).

74. Fijał-Kirejczyk I, Jaskóła M, Korman A, et al. L-subshell ionization of heavy elements by S ions with energy of 0.4-3.8 MeV/amu. Nuclear Instruments and Methods in Physics Research, Section B: Beam Interactions with Materials and Atoms 266 (2008): 2255-2258.

Ejeh E, et al., J Biotechnol Biomed 2024
DOI:10.26502/jbb.2642-91280170

75. Bhattacharya D, Sarkar M, Chatterjee MB, et al. L-subshell ionization cross sections in gold and bismuth by 3.6—9.5-MeV carbon and 4.0—7.2-MeV oxygen ious. Phy Rev A 49 (1994): 4616-4623.

76. Sarkadi L, Mukoyama T. Measurements of L X-ray production and subshell ionisation cross sections of gold by light- and heavy-ion bombardment in the energy range 0.4-3.4 MeV. J Phys B: Atom Mol Phys 13 (1980): 2255-2268.

77. Sarkadi L, Mukoyama T. Systematic study of helium-induced L shell ionization cross sections. Nuclear Inst and Methods in Physics Research B 61 (1991): 167-17.

78. Bang J, Hansteen M. Danske Vidensk. Selsk., Mnr.-Fys. Meddr. 31 (1959): 1-43.

79. Hansteen JM. The SCA description of inner-shell coulomb ionization and associated phenomena. Nuclear Inst and Methods in Physics Research B 42 (1989): 426-435.

80. OPPENHEIMER JR. On the quantum theory of the free electron laser. Optica Acta 31 (1928): 267-270.

81. Lapicki G, Losonsky W. Electron capture from inner shells by fully stripped ions. Journal of Chemical Information and Modeling 53 (1977): 1689-1699.

82. Pauli M, Rosel F, Trautmann D. Electronic relativistic effects in the semiclassical theory of K-shell ionisation', Journal of Physics B: Atomic and Molecular Physics 11(1978): 2511-2526.

83. Amundsen PA. Coulomb deflection effects in ion-induced K-shell ionisation. Journal of Physics B: Atomic and Molecular Physics 10 (1977): 2177-2187.

84. Jakob A, Trautmann D, Roesel F, et al. Wave Function Effects in Inner Shell Ionization. Nuclear Instruments and Methods in Physics Research, Section B: Beam Interactions with Materials and Atoms 232 (1984): 218-226.

85. Trautmann, Rösel F. On the semiclassical description of Coulomb ionization of inner shells. Nucl Instrum and Methods 169 (1980): 259-272.

86. Choi B, Merzbacher E, Khandelwal GS. Tables for born approximation calculations of l-subshell ionization by simple heavy charged particles. Atomic Data and Nuclear Data Tables 5 (1973): 291-304.

87. Phinney LC, Duggan JL, Lapicki G, et al. Thorium and uranium M-shell x-ray production by 0.4–4.0 MeV protons and 0.4–6.0 MeV helium ions. J Phys B At Mol Opt Phys 42 (2009): 085202.